ACCEPTED VERSION

http://hdl.handle.net/2440/118286

Bolted Joint Integrity Monitoring with Second Harmonic Generated by Guided Waves

Yi Yang, Ching-Tai Ng[*]

School of Civil, Environmental and Mining Engineering, The University of Adelaide, Adelaide, SA 5000, Australia

Andrei Kotousov

School of Mechanical Engineering, The University of Adelaide, Adelaide, SA 5000, Australia

Abstract

In this study, the second harmonic generation (SHG) due to the contact nonlinearity caused by bolt loosening is studied experimentally and numerically using three-dimensional (3D) explicit finite element (FE) simulations. In particular, it is demonstrated that the magnitude of the SHG normally increases with the loosening of the bolted joint, and there is a reasonable agreement between the numerical simulations and experimental results. The FE model, which was validated against experimentally measured data, is further utilised to investigate an important practical situation when a loosened bolt is weakened by fatigue cracks located at the edge of the hole. The numerical case studies show that the contact nonlinearity and the change of the behaviour of the SHG with the tightening level are very different to the corresponding results with the fatigue cracks. This identified difference in the SHG behaviour can serve as an indicator of the bolted joint integrity, and thus to provide early warning for engineers to make decision on necessity of carrying out further safety inspections. Overall, the findings of this

---

[*] Corresponding author. Email: alex.ng@adelaide.edu.au

study provide improved physical insights into SHG for bolt loosening, which can be used to further advance damage detection techniques using nonlinear guided waves.

Keywords: Bolt loosening, guided waves, second harmonic generation, contact nonlinearity, fatigue crack, torque loss, structural health monitoring, bolted joint

1. Introduction

In last two decades, different non-destructive evaluation (NDE) techniques and damage detection methods[1] have been developed and applied to detect damages, e.g., visual inspection[2], eddy current[3], thermography[4], conventional ultrasonic[5], vibration techniques[6-8] and guided wave technique[9,10], etc. Among these methods, guided wave inspection has proven its advantages over the conventional NDE techniques and damage detection methods[11], such as its ability to inspect large area, capability of evaluating inaccessible structural components in structures, high sensitivity to small damages, and potential to develop online structural health monitoring (SHM) system through transducer network.

1.1. Guided waves for damage detection

Guided waves have attracted significant research interest due to its ability to propagate in different types of structures, such as beam[12], rod[13], plate[14-16] and pipe[17,18]. In recent years, many studies using linear or nonlinear guided waves have been carried out and they focused on different damage types and materials[19,20]. For linear guided wave, Sohn[21] used mode conversion technique to detect a notch on an aluminium plate. A reference-free damage detection method was introduced. Santos *et al.*[22] employed guided waves to characterize the interface texture of two-layer concrete slabs. Numerical simulation studies were carried out to investigate the feasibility and performance of the proposed method.

As compared with linear features of guided waves, the nonlinear features have attracted increasing attention due to its ability to detect both contact nonlinearity of cracks[23] and plasticity driven damages[24,25] at impercipient level. In general, the linear features of guided waves usually require reference data to extract the damage related information for damage detection. But the varying operational[26,27] and environmental condition[28,29] can significantly affect the accuracy of extracting the damage related information using the reference data. Different to linear features of guided waves, the nonlinear features are potential to be developed as a reference free damage detection technique[30].

Pruell *et al.*[31] studied the plasticity driven nonlinearity using the second harmonic generation (SHG) due to phase and group velocity matching of the first and second symmetric modes of Lamb wave. They found that with larger plastic deformation, the acoustic nonlinearity induces larger magnitude of higher harmonic. Soleimanpour *et al.*[32] numerically and experimentally investigated the SHG due to contact nonlinearity at delamination in laminated composite beam. Various damage scenarios about different delamination layers and sizes were considered in their study. Lim *et al.*[33] investigated the binding conditions for nonlinear guided wave generation. Their study considered both propagating wave and stationary vibration. An aluminium plate specimen with a fatigue crack was used in their experimental studies. The binding conditions to generate modulated guided wave signals and sidebands were studied using both high and low frequency excitations. Yang *et al.*[34] investigated the SHG of the Lamb waves at fatigue crack in aluminium plate. 3D FE simulations and experiments were carried out to gain physical insights into the SHG phenomenon at fatigue crack. They also extended the work to investigate the SHG under practical situations, such as effect of the crack opening under applied loading condition and incident wave angle on the SHG[35].

1.2. Detection of damage for bolted joints

Research on detection of contact-type damage with nonlinear guided waves has attracted significant attention in recent years. The contact-type defects such as fatigue crack or delamination, are sources of contact nonlinearity phenomena contributing the generation of the second order harmonics. Another common type of structural deficiency related to the contact nonlinearity is the loosening of a bolted joint. The bolted joint is an essential component in many structures, e.g., wind turbines, bridges and framed buildings. Bolt loosening is one of the major concerns for engineers[36].

The loss of torque in one or more bolts can significantly decrease fatigue life of bolted joints[37,38]. When bolt loosening occurs, the friction between the lapped areas of the joint reduces due to the decrease of the clamping force contributed by the bolts. In this situation, the applied load is directly transferred from one plate to the other through the contact area between the bolt and plates and this causes a stress concentration at the edge of the bolt hole[39]. When the structure is subjected to alternating loading, fatigue cracks can be developed at the edge of the bolt hole. Therefore, reliable and cost efficient non-destructive techniques capable to detect the bolt loosening and fatigue crack of bolted joint at critical load bearing structural components are essential for safety and integrity of a wide range of engineering structures.

1.2.1. Linear guided wave for detecting bolt loosening

There were a number of studies focused on detection of bolt loosening using linear guided waves. Wang *et al.*[40] investigated the relationship between the signal energy and applied torque levels at bolted connections. It was found that the wave energy propagated through the connection increases with the applied torque. In another paper, Wang *et al.*[41] proposed a time reversal method using the linear guided wave signals to monitor the bolted joints. Experimental study was carried out to investigate the relationship between the peak amplitudes of the time

reversal focused signal and the bolt preload. However, the linear guided waves have some issues that need to be addressed before it can be applied in practical situations. For examples, as mentioned before, the linear features of guided waves are sensitive to the temperature change[42,43]. Moreover, the boundary reflection of the linear guided waves within the lapped areas at the bolted connection would affect the linear features utilised in the detection algorithms of bolt loosening[44].

1.2.2. Nonlinear guided wave for detecting bolt loosening

Different to linear features, the nonlinear features of guided waves are more robust for structures with complex geometry[45] and under varying temperature condition. One of the most commonly used nonlinear features of guided waves is SHG due to the contact nonlinearity. This phenomenon can be described by Contact Acoustic Nonlinearity (CAN)[46]. When guided wave interacts with a contact-type of damage, such as fatigue crack and loosen bolt, repetitive collisions between contact surfaces occurs. During the collisions, the compressive and tensile pressure of the wave closes and opens the contact surfaces, respectively. However, only the compressive pressure of the wave can transmit through the closed contact surfaces. Therefore, after the incident wave interacting with the contact surfaces, the wave shape is rectified nearly half-wave. The higher harmonics are generated due to this nonlinear waveform distortion. This phenomenon is schematically illustrated in Figure 1.[25]

[Figure 1: Schematic diagram of contact nonlinearity at contact surfaces]

Biwa *et al.*[47] used bulk waves to study the SHG due to the variation of contact pressure between two separate aluminium blocks at the contact interface. They found that the amplitude of the second order nonlinear parameters decreases with the contact pressure. The study

suggests that the SHG of the bulk wave is sensitive to the change of contact pressure between two contact surfaces. The bolt loosening causes a loss of contact pressure at the interface of a bolted joint so the nonlinear features can be used to detect bolt loosening at the bolted connections. In the study carried out by Lee and Jhang[48], although it focused on detecting the fatigue crack in an aluminium block using the SHG of ultrasonic bulk wave, they also experimentally investigated the closing effect of the fatigue crack. They found that the magnitude of the applied pressure is inversely proportional to the magnitude of the SHG. This means that the contact nonlinearity reduces with the increasing torque contributed by the bolt, and vice versa. However, the safety inspection using bulk wave is only able to provide a localised assessment for structures. In practical situation, most of the structures have inaccessible areas. It is difficult to inspect these inaccessible areas using the bulk wave. Different to bulk wave, guided wave propagates along the structure, which can cover a large inspection area and can be used to inspect inaccessible locations.

In the literature, there were several studies investigated the feasibility of using the SHG of guided waves to detect the bolt loosening. For example, Amerini and Meo[49] studied the effect of bolt loosening and tightening at the bolted connection using nonlinear guided waves. They showed that the spectral amplitude difference between the carrier frequency (A_1) and the second harmonic frequency (A_2) at bolt loosening condition is much lower than that at tightening condition. They proposed a hyperbolic tangent function to predict the spectral amplitude difference for different magnitudes of the torque applied at the bolt. However, defining the damage index related to A_1 may involve some problems, as the wave reflection and contact pressure would significantly affect the amplitude of the linear wave[44]. They also suggested that there is no clear change of damage index when the magnitude of the applied torque increases beyond around 6 Nm, which means the proposed damage index may not be able to provide early detection of bolt loosening.

This study is different from the previous research efforts published in the literature. It deals with the characteristics of SHG when a loosened bolt connection is weakened by fatigue cracks. The latter represents a typical practical situation, which is of a main concern for engineers as discussed above. The current study provides a comprehensive numerical and experimental insights into the complex contact nonlinearity caused by combination of bolt loosening and fatigue cracks. These insights could further advance the non-destructive techniques for integrity monitoring of the bolted joints using nonlinear guided wave.

The paper is organized as follows. Sections 2 and 3 describe the setup of experiment and three-dimensional (3D) finite element (FE) model of bolted connections, respectively. Then, the experimental and FE simulation results are discussed in detailed in Section 4. This section employs the experimentally verified 3D FE model to investigate the SHG when a loosened bolt is weakened by fatigue crack located at the edge of the bolt hole. Different levels of bolt loosening are investigated using the experimentally verified 3D FE model. Finally, conclusions are drawn in Section 5.

2. Experiment

2.1. Experimental specimens

The experimental study considered a single-lap connection and T-joint connection as shown in Figures 2a and 2b, respectively. The lengths of the specimens are relatively short so that it can also demonstrate the proposed nonlinear guided wave approach is applicable to the situation having wave reflections from the boundaries, which has been demonstrated that it is hard to be handled using linear guided wave approach in Section 1.2.1. The first specimen is a single-lap connection as shown in Figure 2a. The specimen consists of two 5 mm thick plates with in-plane dimension of 50 mm $\times$ 24 mm. The second specimen is a T-joint connection (Figure 2b), which consists two 5mm thick plates with in-plane dimensions of 70 mm $\times$ 24 mm and 24 mm $\times$ 24 mm, respectively. Both specimens are made of G250 mild steel and the material properties

are shown in Table 1. A M10 steel bolt was used to connect the two steel plates of each specimen. A torque wrench with electronic readings was used to tighten the bolt and measure the magnitude of the applied torque. The minimal torque that can be measured by the torque meter is 6.8 Nm and the sensitive of the measurement is ±2%.

[Figure 2: a) Single-lap joint and b) T-joint specimen used in experiment]

[Table 1: Material properties of the G250 mild steel plate]

[Table 2: Material properties of the Ferroperm Pz27 Piezoceramic disc]

2.2. Actuating and sensing guided wave

Rectangular piezoceramic transducers (Ferroperm Pz27) with 6 mm × 12 mm in-plane dimension and 2 mm thickness were bonded to the surface of the plate by conductive epoxy. These piezoceramic transducers were used to excite and receive the wave signals. The material properties of the transducers are listed in Table 2. Figure 3 shows a schematic diagram of the experimental setup. A computer controlled signal generator (NI PIX-5412) was used to generate the excitation signal, which was a narrow-band 10-cycle sinusoidal tone burst pulse modulated by a Hanning window. 50 kHz and 200 kHz excitation frequencies were considered in this study. The excitation signal has a peak-to-peak output voltage of 10 V and was amplified by a factor of four using an amplifier (KROHN-HITE 7500) before it was sent to one of the transducers. The other transducer was used to measure the wave signals on the specimen. The measured signals were then digitized by a data acquisition system (NI PXIe-5105). The quality of the measurements was improved by averaging the signals with 64 acquisitions.

[Figure 3: Schematic diagram of experimental setup]

2.3. Experimental observation of SHG due to bolt loosening

The torque level was increased stepwise from 8 Nm to 20 Nm in steps of 2 Nm. The experimental process was repeated independently 10 times for each specimen and the excitation frequency, respectively. The measured 200 kHz wave signal at the single-lap joint specimen with torque equals to 8 Nm is shown in Figure 4. Figures 4a and 4b show the measured time-domain signal and the frequency-domain signal processed using fast Fourier transform, respectively. As shown in Figure 4b, besides the SHG at frequency $2f$, there are also other higher order harmonics, e.g., third ($3f$) and fourth ($4f$) harmonics. But the focus of the current study is to investigate the feasibility of using SHG to detect bolt loosening.

The extracted SHG amplitude, A_2, against the magnitude of applied torque for all 10 tests are summarised in Figures 5 and 6. Figures 5 and 6 show the averaged results for the single-lap joint and T-joint, respectively. The error bars are calculated at different applied torque magnitudes (levels).

[Figure 4: Measured a) time-domain and b) frequency-domain signals from single-lap joint specimen for 200 kHz excitation frequency and 8 Nm torque]

The results indicate that the averaged SHG amplitude generally decreases with the increasing applied torque. For cases considering single-lap joint and T-joint with 50 kHz excitation frequency (Figure 5a and 6a), comparing to loosened bolt, the SHG amplitude decreases by more than 60% when the bolt is tightened. When the 200 kHz excitation is used, the SHG amplitude of the tightened bolt is only reduced by about 10% at the bolt loosening condition (Figure 5b and 6b). The results also demonstrate that the magnitude of SHG for the

single-lap joint at bolt loosening condition are larger than that for the T-joint, especially for the case when 50 kHz incident wave is used.

[Figure 5: Averaged SHG amplitude against applied torque for the single-lap joint specimen with error bars for a) 50 kHz, and b) 200 kHz excitation frequency]

[Figure 6: Averaged SHG amplitude against applied torque for the T-joint specimen with error bars for a) 50 kHz, and b) 200 kHz excitation frequency]

Below are possible reasons that contribute to the observed features of the SHG behaviour with the change of the torque level, as well as the variation of the results.

1) The wave in the single-lap joint is transmitted through the bolted area and interacts with the two plates. The contact behaviour at the interface has a significant impact on the wave signals. Between each individual test, the contact characteristic at the interface can be quite different, especially when the bolt is loosened. Thus, the amplitude of the SHG has larger fluctuation at the bolt loosening condition. For the T-joint specimen, the wave energy can pass through the bolted area without any interaction at the interface, therefore, the amplitude of the SHG is smaller than that in the single-lap joint specimen at the bolt loosening condition. Also, the variation of the SHG for the single-lap joint is larger than that for the T-joint.

2) The actual contact pressure at the bolted joint does not vary linearly with the applied torque. In each time of the torque is applied in the experiment, there may be a small slip between the washer and plate, the top plate and base plate, and the bolt and washer. Therefore, this changes the effective contact area and would result in different clapping behaviours and magnitudes of friction force.

3) As the bolt hole is normally designed to be slightly larger than the diameter of the thread, the gap and the contact area between the bolt thread and the plates can vary in different tests. Obviously, this can affect the measured amplitude of the SHG induced by contact nonlinearity.

4) The measurement error of the torque meter and rounding error of data acquisition process could influence the variation of the SHG in the measured data.

3. Three-dimensional Explicit Finite Element Simulations

3.1. FE modelling of bolt loosening

The configurations utilized in the experimental study were modelled using 3D explicit FE method. ABAQUS/CAE was used to model the specimen geometry and loading/contact conditions as shown in Figure 1. In the FE model, only the plates and washer of the specimens were modelled and the effect of the bolt tightening was modelled by applying pressure on the washer. The schematic diagrams of the FE models are shown in Figure 7. The dimensions of the FE models are exactly the same as those specimens used in the experiment. The specimens were modelled using 8-node linear brick elements with reduced integration (C3D8R). Hourglass control was used to ensure the stability of the simulations. The in-plane dimension of the element is 0.4 mm × 0.4 mm. This ensures that there are at least 20 elements in the wavelength of the incident wave and second harmonic wave. The thickness of the element is 0.5 mm so there are ten elements in the thickness direction of the plates.

[Figure 7: Schematic diagram of the FE model for the a) single-lap joint and b) T-joint]

The interaction between the plates at the joint location was modelled by 'hard' normal interaction and frictional tangential interaction with friction factor equals to 0.5[50]. The

excitation signal and excitation frequencies are the same as those used in the experiment, which are narrow-band 10-cycle sinusoidal tone burst pulse modulated by a Hanning window, and at 50 kHz and 200 kHz. The guided wave was generated by applying nodal displacement at the top edge of the piezoceramic transducer, and the propagating waves were measured using the strain of an element. The bolt tightening condition was modelled by applying evenly distributed pressure on the washers. The magnitude of the pressure is determined by[36]:

$$P = \frac{T}{kdA} \tag{1}$$

where P is the pressure, T is torque applied on the bolt, k is the torque coefficient, d is the nominal diameter of the bolt, and A is the area of washer. $k = 0.2$ is usually used for steel bolts[36]. In this study, the pressure on the washer is applied through a quasi-static loading using 'smooth step' in ABAQUS to avoid inducing any shock wave on the specimens due to sudden loading condition. The FE simulation of the bolt loosening includes two steps, 1) the washers are loaded using dynamic explicit procedure with smooth loading to avoid the transient effect in applying the pressure, and then 2) guided waves are excited and SHG is induced due to the interaction between the incident wave and the joint with bolt loosening.

4. Results and Discussions

4.1. FE calculated and experimentally measured SHG due to bolt loosening

Figure 8 shows the FE calculated and experimentally measured amplitude of SHG, which is normalized by the averaged value of A_2 at different torque levels of the corresponding case. The averaged experimental results of the 10 individual tests are also shown in Figure 6. It is evident that, for both excitation frequencies, the amplitudes of the SHG decrease with the increasing torque. Meanwhile, the variation and trend of the experimental and FE calculated

results are very similar. The results indicate that the FE model is capable to provide a reasonable prediction of the SHG for the bolt with different levels of the applied torque.

[Figure 8: FE calculated and experimentally measured normalised second harmonic amplitude for single lap joint using a) 50 kHz and b) 200 kHz excitation frequency; and T-joint using c) 50 kHz and d) 200k Hz excitation]

4.2. Effect of excitation frequency

As shown in the experimental and FE results, the selection of excitation frequency plays an important role in detecting the bolt loosening level. Also, the wave modes of the guided wave generated by the piezoceramic transducer highly depend on the excitation frequency. In this section, the wave motion of the excited guided wave is investigated to determine the efficiency of different wave modes in SHG due to bolt loosening.

In the literature, it has been shown that the 3D FE simulation can accurately predict the linear wave propagation in both isotropic and composite materials[52,53]. This study employs the 3D FE model to investigate the 50 kHz and 200 kHz linear wave propagation to reveal the dominant wave mode at each excitation frequency. The model has the same thickness, width, material properties and distances between actuator and measurement points as the FE models described in Section 3.1, except that the length of the model is extended to 1 m to avoid the wave reflected from the boundaries. The model is shown in Figure 9. Since the guided wave propagation is a local phenomenon, the only difference between the extended length model and the model shown in Figure 7 is the wave reflected from the boundaries.

[Figure 9: 3D FE model for studying the in-plane and out-of-plane deformation of the guided wave propagation]

Both the in-plane and out-of-plane displacements are measured at the measurement point as shown in Figure 10. Figure 10 shows that the out-of-plane displacement of the 50 kHz guided wave is at least two times larger than that of 200 kHz guided wave. This is because the dominated wave mode is the fundamental anti-symmetric mode (A_0) at 50 kHz. However, both 50 kHz and 200 kHz guided waves have very similar magnitude of in-plane displacement.

Based on the results presented in Section 4.1, the A_0 guided wave, which has dominant out-of-plane motion, is more sensitive to the SHG due to changes of the contact pressure at the bolted joint. This is consistent with the findings in the previous research[49]. This explains that when 200 kHz is chosen as the excitation frequency, the amplitude reduction of the SHG with the increasing torque is less significant than that of 50 kHz guided wave.

[Figure 10: FE calculated in-plane and out-of-plane displacement at a) 50 kHz and b) 200 kHz excitation frequency]

4.3. Effect of fatigue cracks at loosened bolts

As discussed in Section 1, fatigue cracks are very common in bolted joints due to cyclic loading of the structure or due to the change of environmental condition. The fatigue crack would enhance the complexity of the contact nonlinearity and guided wave interaction with the overlapped area at the bolted joints, and hence, affecting the behaviour of SHG. It has been demonstrated that the 3D FE model is capable of predicting the SHG features due to the interaction of low-frequency guided wave and fatigue crack[34]. The similar methodology will be utilized in the current numerical study.

A 3D FE model containing two 3 mm long fatigue cracks at two sides of the bolt hole is considered in this section. The fatigue cracks are modelled by duplicating the FE nodes at the crack surface areas and the locations are shown in Figure 11. The measurement is also taken

at the same location as the FE model shown in Figure 7 in Section 3.1. 'Hard' contact is defined between the crack surfaces and a friction factor of 1 is used to model the frictional interaction between the crack surfaces, which also takes into account the rough fatigue crack surfaces in real situation[34]. The features of the SHG at the bolted joint with fatigue cracks are observed at different torque levels.

[Figure 11: 3D FE model of a) single lap joint and b) T-joint with fatigue cracks at the bolt hole]

Figure 12 shows the ratio of the second harmonic amplitude obtained from the FE model with the fatigue cracks to the second harmonic amplitude obtained from the FE model of the tightened bolt (intact specimen and the value of the torque for intact bolted joint is 20 Nm), and it is defined as

$$r = \frac{A_2}{A_{2,T=20\,Nm}} \tag{2}$$

where A_2 is the second harmonic amplitude of the FE model with the fatigue cracks, and $A_{2,T=20Nm}$ is the second harmonic amplitude of the intact bolted joint (tightened bolt) when the torque is 20 Nm.

[Figure 12: Second harmonic amplitude ratio of a) single-lap joint and b) T-joint]

The results of the single-lap joint with fatigue cracks are shown in Figure 10a. The second harmonic amplitude ratio increases with the applied torque. When the bolt is loosened, part of the wave energy is transferred from the fundamental frequency to second harmonic frequency due to "the breathing phenomenon" of the wave-crack interaction. But the second harmonic wave generated at the fatigue cracks cannot propagate through the joint with the loosened bolt.

While the bolt is tightened, second harmonic wave due to the fatigue cracks can travel through the bolted joint, and most of the wave energy is transferred from the fundamental frequency to the second harmonic frequency due to contact nonlinearity at the fatigue cracks. However, as described in Sections 4.1, at the bolted joint, the amplitude of SHG decreases when the applied torque increases. So, in this case, the increase of A_2 due to the fatigue cracks is more significant than the decrease of A_2 due to tightened bolt.

For the T-joint (Figure 10b), when 200 kHz guided wave is used, the variation of the amplitude ratio is similar to that of single-lap joint. In contrast, when 50 kHz guided wave is used, the second harmonic amplitude ratio decreases when the torque increases. The reason may be that, for the T-joint, the fatigue cracks is located at the same plate of the actuator and measurement point, so the generated second harmonic wave due to fatigue crack is still able to propagate through the bolted joint even the bolt is loosened. For the 50 kHz guided wave, when the magnitude of the applied torque increases, the variation of the second harmonic amplitude ratio is dominated by the contact nonlinearity at the overlapped area of the two plates.

For the results in Figures 8 and 12, when 200 kHz guided wave is used, the variation of second harmonic amplitude due to increasing torque shows an opposite trend when the fatigue cracks are modelled as compared with the results of the FE model without the fatigue cracks. Meanwhile, when 50 kHz guided wave is used as the incident wave, the variations of the second harmonic amplitude ratio for the single-lap joint with and without the fatigue cracks also show an opposite trend. As compared, for the T-joint, the trend and variation of the second harmonic ratio for the FE models with and without the fatigue cracks are similar to each other. It is possible to use 200 kHz guided wave to detect the damage and distinguish the damage type at the bolted joint by continuous monitoring the second harmonic amplitude. When incident wave is generated at 50 kHz, it is only possible to detect damages and distinguish the damage type at the single-lap joint.

5. Conclusions

In this study, SHG induced by the contact nonlinearity due to the bolt loosening in single-lap joint and T-joint has been studied in detail. It has been demonstrated that the FE and experimental results have the same tendency that the value of the second harmonic amplitude for the tightened bolts is smaller than that for the loosened bolts. The study has shown that the use of the guided wave mode with dominated out-of-plane displacements (e.g. A_0 guided wave) can result in much more distinctive reduction in the second harmonic amplitude and also less variation as compared to the case when the in-plane displacements dominated guided wave mode is used (e.g. the fundamental symmetric mode (S_0) guided wave).

The numerical case study using 3D explicit FE simulations has been carried out to investigate the combined effect of bolt loosening and fatigue crack at bolt hole. Different trends and variations of the second harmonic amplitude against the applied torque and different excitation frequencies have been observed. The results have been compared with the corresponding cases without fatigue cracks. The results have indicated that it is possible to distinguish the situation when the joint with loosened bolt is weakened by the fatigue cracks.

The current study focuses on the bolted joint with a single bolt. But in the practical condition, the structure component can contain a group of bolts. Future studies can be carried out on full-scale structural components and bolted joint within a group of bolted connections. This will further justify the feasibility of using the SHG in detecting and distinguishing the bolt loosening with and without the fatigue cracks in practical situation.

Acknowledgement

References

1. Gros X. NDT Data Fusion, Elsevier, 1996

2. Komorowski JP and Forsyth DS. The role of enhanced visual inspections in the new strategy for corrosion management. *Aircr Eng Aerosp Technol* 2000; 71(1): 5-13

3. Lepine BA, Giguere JSR, Forsyth DS, Chahbaz A, Dubois JMS. Interpretation of pulsed eddy current signals for locating and quantifying metal loss in thin skin lap splices. *AIP Conf Proc* 2002; 615(1): 415–422

4. Hiasa S, Birgul R and Catbas FN. Infrared thermography for civil structural assessment: demonstrations with laboratory and field studies. *J Civil Structl Health Monit* 2016; 6: 619-636.

5. Schmerr LW and Song JS. Ultrasonic nondestructive evaluation systems, Springer, 2007

6. Carden EP and Fanning P. Vibration based condition monitoring: a review. *Struct Health Monit* 2004; 3: 355–377.

7. Khoo LM, Mantena PR and Jadhav P. Structural damage assessment using vibration modal analysis. *Struct Health Monit* 2004; 3: 177–194.

8. Hamey CS, Lestari W, Qiao P, *et al*. Experimental damage identification of carbon/epoxy composite beams using curvature mode shapes. *Struct Health Monit* 2004; 3: 333–353.

9. Giurgiutiu V and Bao J. Embedded-ultrasonics structural radar for in situ structural health monitoring of thin-wall structures. *Struct Health Monit* 2004; 3(2): 121-140.

10. He S and Ng CT. A probabilistic approach for quantitative identification of multiple delaminations in laminated composite beams using guided wave. *Eng Struct* 2016; 127: 602-614.

11. Rose LJ. A baseline and vision of ultrasonic guided wave inspection potential. *J Press Vess Tech* 2002; 124: 273-282

12. He S and Ng CT. Guided wave-based identification of multiple cracks in beams using a Bayesian approach. *Mech Syst Sig Process* 2017; 84: 324-345.

13. Raisutis R, Kazys R, Zukauskas E, Mazeika L and Vladisauskas A. Application of ultrasonic guided waves for non-destructive testing of defective CFRP rods with multiple delaminations. *NDT E Int* 2010; 43: 416–24.

14. Ng CT. A two-stage approach for quantitative damage imaging in metallic plates using Lamb waves. *Earthqu Struct* 2015; 8: 821–41.

15. Cho H and Lissenden C. Structural health monitoring of fatigue crack growth in plate structures with ultrasonic guided waves. *Struct Health Monit* 2012; 11: 393–404.

16. Haynes C and Todd M. Enhanced damage localization for complex structures through statistical modelling and sensor fusion. *Mech Syst Signal Pr*ocess 2015; 54–55: 195–209.

17. Lowe MJS, Alleyne DN and Cawley P. Defect detection in pipes using guided waves. *Ultrasonics* 1998; 36: 147–154.

18. Lovstad A and Cawley P. The reflection of the fundamental torsional mode from pit clusters in pipes. *NDT&E Int* 2012; 46: 83–93.

19. Aryan P, Kotousov A, Ng CT and Cazzolato BS. A baseline-free method and non-contact method for detection and imaging of structural damage using 3D laser vibrometry. *Struct Contr Health Monitor* 2017; 24: e1894.

20. Mohseni H and Ng CT. Rayleigh wave propagation and scattering characteristics at debondings in fibre-reinforced polymer-retrofitted concrete structures. *Struct Health Monit* 2018; https://doi.org/10.1177/1475921718754371

21. Sohn H. Reference-free crack detection under varying temperature. *KSCE J Civil Eng* 2011; 15: 1395-1404.

22. Santos P, Julio E and Santos J. Towards the development of an in situ non-destructive method to control the quality of concrete-to-concrete interfaces. *Eng Struct* 2010; 32: 207-217.

23. He S and Ng CT. Modelling and analysis of nonlinear guided waves interaction at a breathing crack using time-domain spectral finite element method. *Smart Mater Struct* 2017; 26 :085002.

24. Bermes C, Kim JY, Qu J and Jacobs LJ. Nonlinear Lamb waves for the detection of material nonlinearity. *Mech. Syst. Sig. Process* 2008; 22: 638-646.

25. Jhang KY. Nonlinear ultrasonic techniques for non-destructive assessment of micro damage in material: A review. *Intern J Precision Eng Manu* 2009; 10: 123-135.

26. Mohabuth M, Kotousov A and Ng CT. Effect of uniaxial stress on the propagation of higher-order Lamb wave modes. *Intern J of Nonlinear Mech* 2016; 86: 104-111.

27. Mohabuth M, Kotousov A and Ng CT. Implication changing loading conditions on structural health monitoring utilising guided waves. Smart Mater Struct 2018; 27: 025003.

28. Konstantinidis G, Drinkwater BW, Wilcox PD. The temperature stability of guided wave structural health monitoring systems. *Smart Mater Struct* 2006; 15: 967–976.

29. Aryan P, Kotousov A, Ng CT, Wildy S. Reconstruction of baseline time-trace under changing environmental and operational conditions. *Smart Mater Struct* 2016; 25: 035018.

30. Soleimanpour R and Ng CT. Locating delaminations in laminated composite beams. *Eng Struct* 2017; 131: 207-219.

31. Pruell C, Kim JY, Qu J and Jacobs LJ. Evaluation of fatigue damage using nonlinear guided waves. *Smart Mater Struct* 2009; 18: 035003.

32. Soleimanpour R, Ng CT and Wang CH. Higher harmonic generation of guided waves at delaminations in laminated composite beams. *Struct Health Monit* 2017; 16: 400-417.

33. Lim HJ, Sohn H and Liu P. Binding conditions for nonlinear ultrasonic generation unifying wave propagation and vibration. *Appl Phys Lett* 2014; 104: 214103.

34. Yang Y, Ng CT, Kotousov A, Sohn H and Lim HJ. Second harmonic generation at fatigue cracks by low-frequency Lamb waves: Experimental and numerical studies. *Mech Syst Signal Process* 2018; 99: 760-773.

35. Yang Y, Ng CT, Kotousov A. Influence of crack opening and incident wave angle on second harmonic generation of Lamb waves. *Smart Mater & Struct* 2018 https://doi.org/10.1088/1361-665X/aab867

36. Caccese V, Mewer R and Vel SS. Detection of bolt load loss in hybrid composite/metal bolted connections. *Eng Struct* 2004; 26: 895-906.

37. Ju SH, Fan CY and Wu GH. Three-dimensional finite elements of steel bolted connections. *Eng Struct* 2004; 26: 403-413.

38. Minguez JM and Vogwell J. Effect of torque tightening on the fatigue strength of bolted joints. *Eng Failure Analy* 2006; 13: 1410-1421.

39. Salih EL, Gardner L, Nethercot DA. Bearing failure in stainless steel bolted connections. *Eng Struct* 2011; 33: 549-562.

40. Wang T, Song G, Wang Z and Li Y. Proof-of-concept study of monitoring bolt connection status using a piezoelectric based active sensing method. *Smart Mater Struct* 2013; 22: 087001.

41. Wang T, Liu S, Shao J and Li Y. Health monitoring of bolted joints using the time reversal method and piezoelectric transducers. *Smart Mater Struct* 2016; 25: 025010.

42. An YK and Sohn H, Instantaneous crack detection under varying temperature and static loading conditions. *Struct Health Monitor* 2010; 17: 730-741.

43. Aryan P, Kotousov A, Ng CT and Cazzolato B. A model-based method for damage detection with guided waves. *Struct Control Health Monitor* 2017; 24: e1884.

44. Bao J and Giurgiutiu V. Effects of fastener load on wave propagation through lap joint. Proc SPIE 2013; 869521.

45. Dutta D, Sohn H, Harries K and Rizzo P. A nonlinear acoustic technique for crack detection in metallic structures. *Struct Health Monit* 2009; 8: 0251-12.

46. Solodv IY, Krohn N and Busse G. CAN: an example of nonclassical acoustic nonlinearity in solids. *Ultrasonics* 2002; 40:621-625.

47. Biwa S, Hiraiwa S and Matsumoto E. Experimental and theoretical study of harmonic generation at contacting interface. *Ultrasonics* 2006; 44: e1319-e1322.

48. Lee TH and Jhang KY. Experimental investigation of nonlinear acoustic effect at crack. *NDT&E Int* 2009; 42: 757-764.

49. Amerini F and Meo M. Structural health monitoring of bolted joints using linear and nonlinear acoustic/ultrasound methods. *Struct Health Monitor* 2011; 10: 659-672.

50. Blau PJ. Friction Science and Technology: from concepts to applications. Boca Raton: CRC Press, 2009.

51. Lu Y, Ye L, Su Z and Yang C. Quantitative assessment of through-thickness crack size based on Lamb wave scattering in aluminium plates. *NDT&E Int* 2008; 41: 59-68.

52. Ng CT. On Accuracy of Analytical Modeling of Lamb Wave Scattering at Delaminations in Multilayered Isotropic Plates. *Intern J Struct Stab Dyn* 2015; 15(8): 1540010.

53. Lowe M, Cawley P, Kao J and Diligent O. The low frequency reflection characteristics of the fundamental antisymmetric Lamb wave a_0 from a rectangular notch in a plate. *J Acoust Soc Am* 2002; 112: 2612-2622.
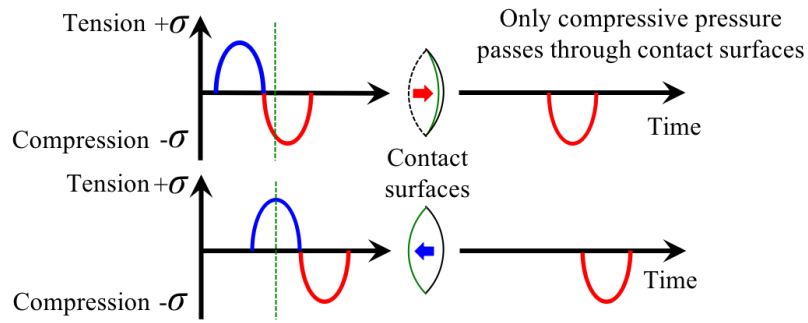
List of Figures

Figure 1: Schematic diagram of contact nonlinearity at contact surfaces
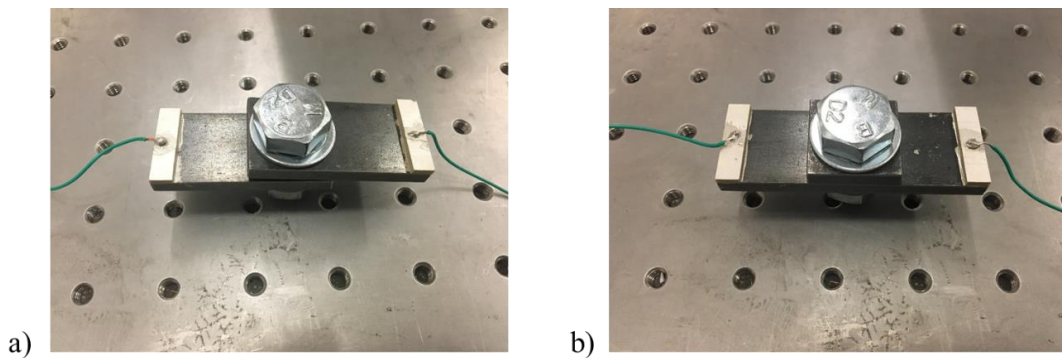

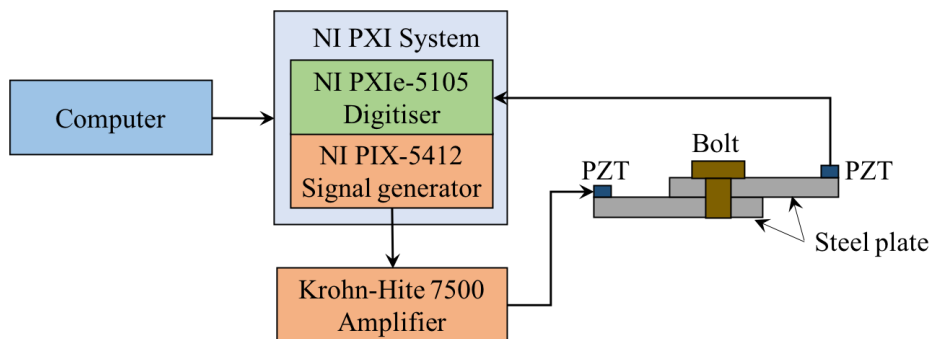Figure 2: a) Single-lap joint and b) T-joint specimen used in experiment

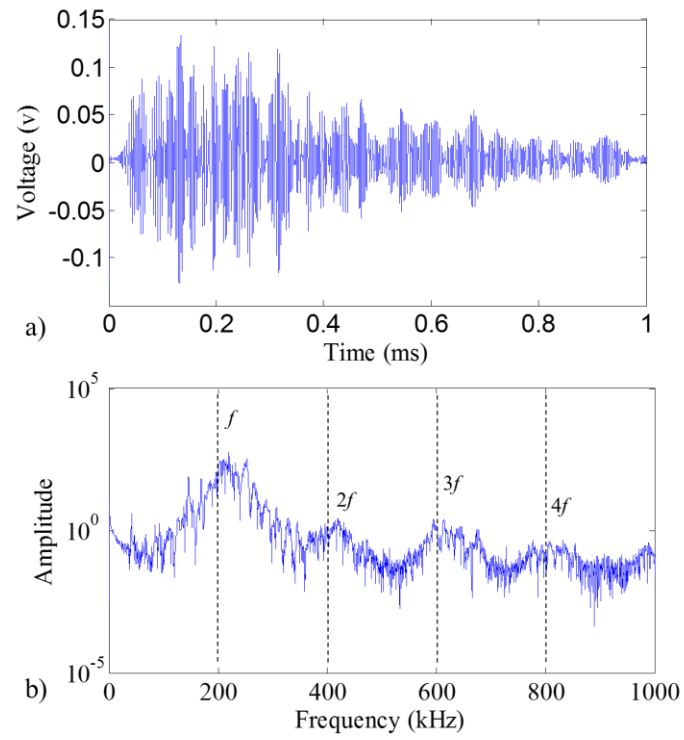Figure 3: Schematic diagram of experimental setup

Figure 4: Measured a) time-domain and b) frequency-domain signals from single-lap joint specimen for 200 kHz excitation frequency and 8 Nm torque
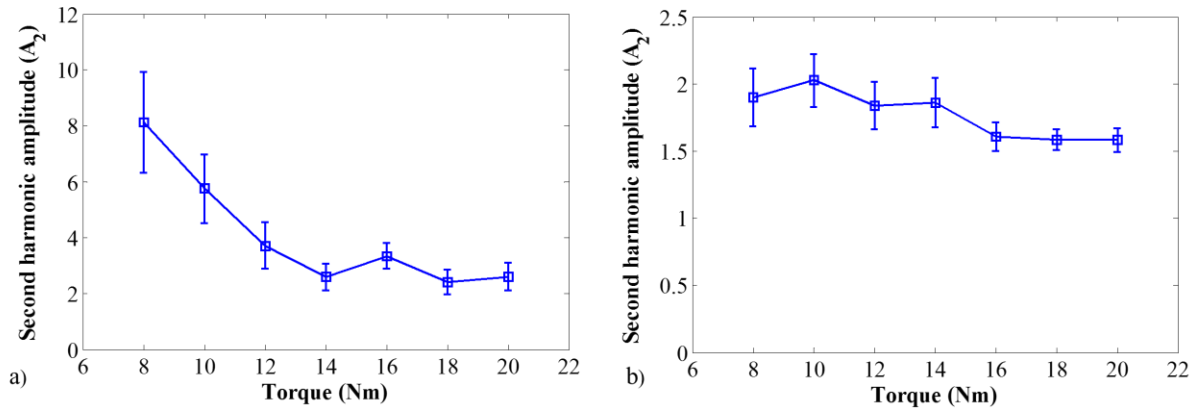
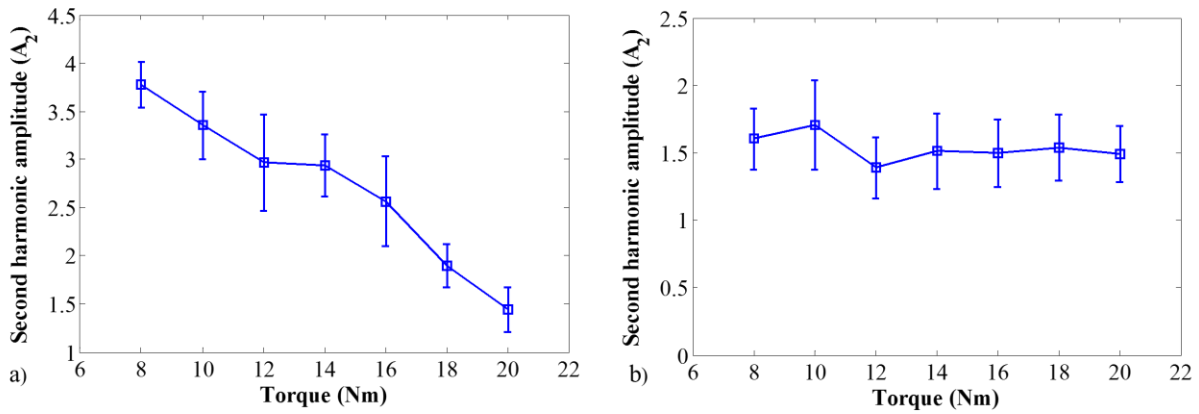Figure 5: Averaged SHG amplitude against applied torque for the single-lap joint specimen with error bars for a) 50 kHz, and b) 200 kHz excitation frequency

Figure 6: Averaged SHG amplitude against applied torque for the T-joint specimen with error bars for a) 50 kHz, and b) 200 kHz excitation frequency
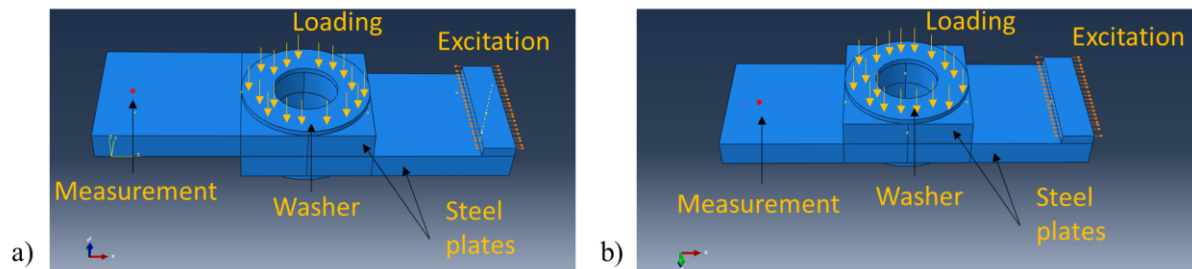
Figure 7: Schematic diagram of the FE model for the a) single-lap joint and b) T-joint
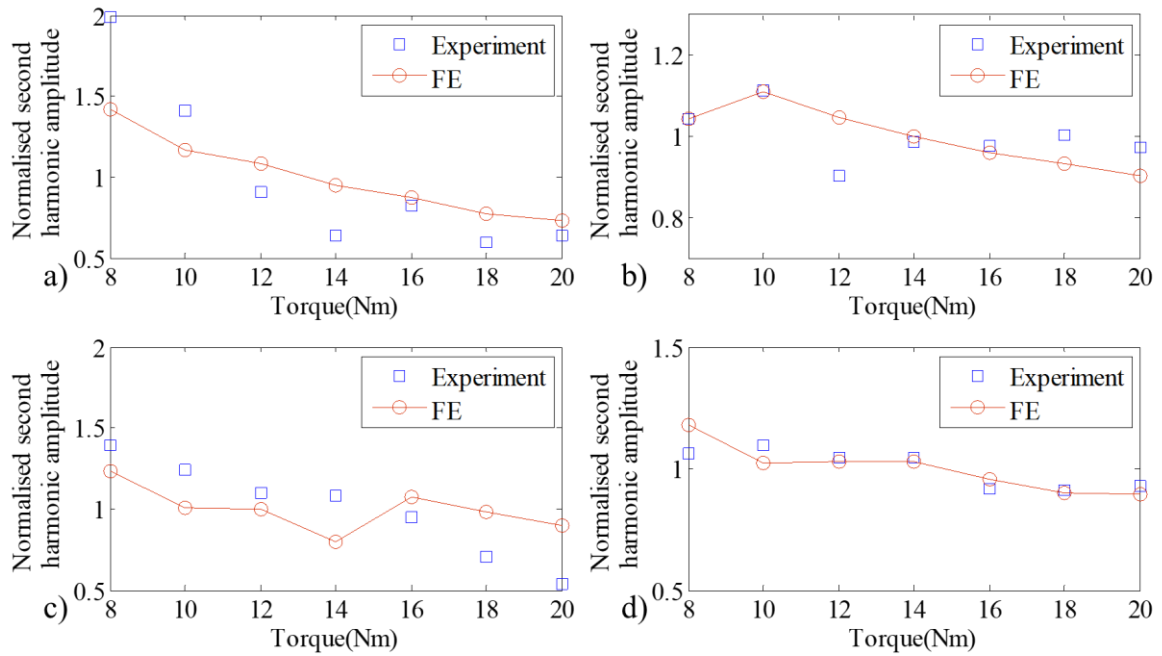
Figure 8: FE calculated and experimentally measured normalised second harmonic amplitude

for single lap joint using a) 50 kHz and b) 200 kHz excitation frequency; and T-joint using c)

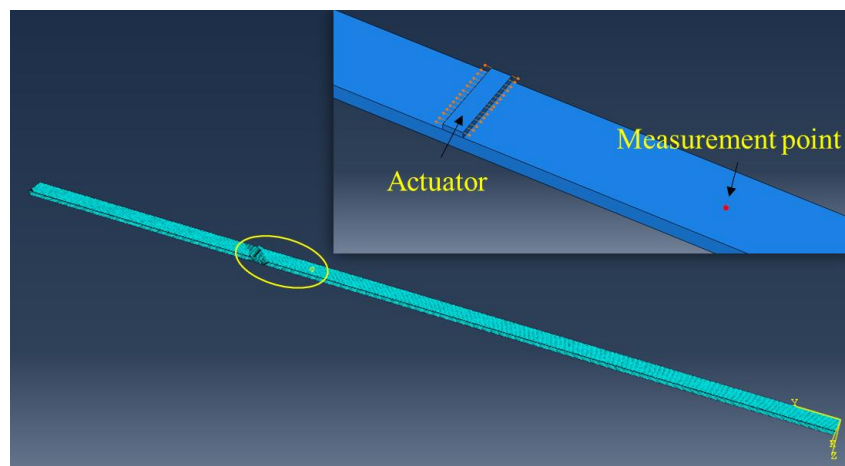50 kHz and d) 200k Hz excitation

Figure 9: 3D FE model for studying the in-plane and out-of-plane deformation of the guided
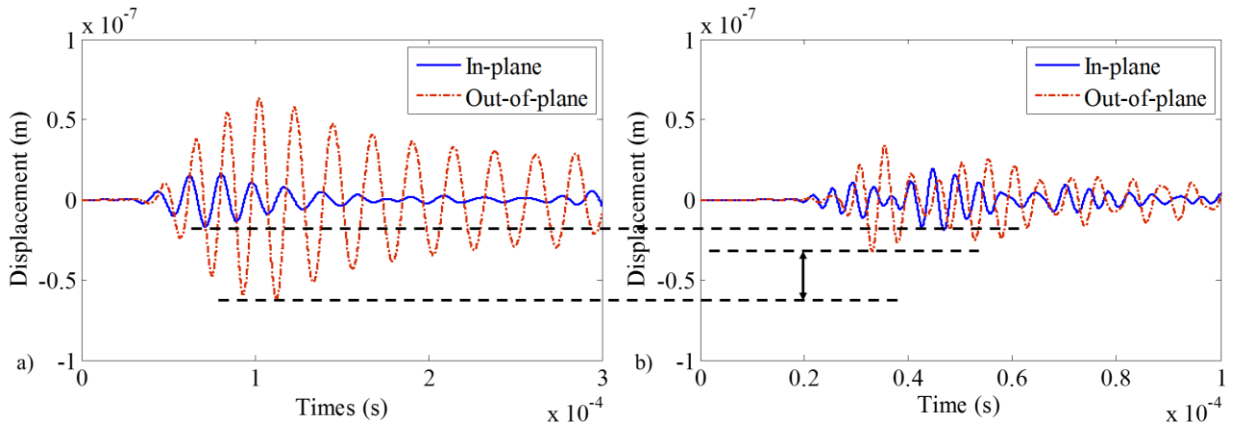
wave propagation

Figure 10: FE calculated in-plane and out-of-plane displacement at a) 50 kHz and b) 200 kHz
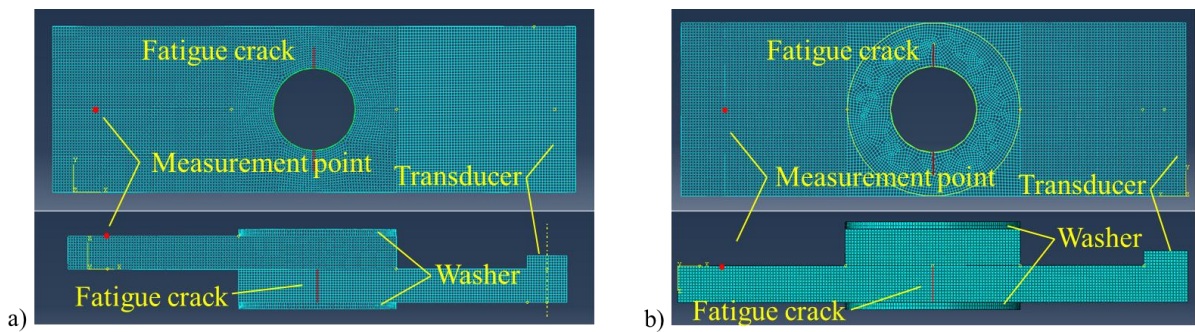
excitation frequency

Figure 11: 3D FE model of a) single lap joint and b) T-joint with fatigue cracks at the bolt
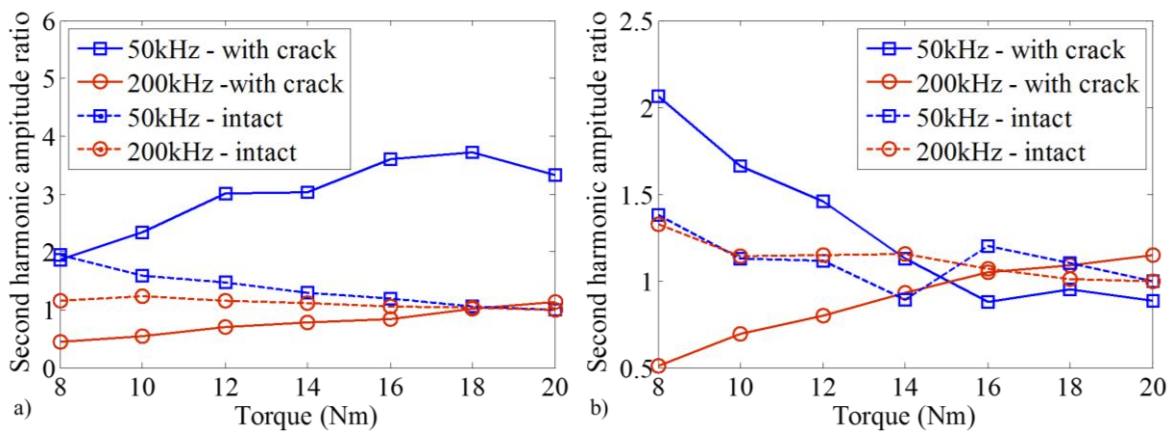
hole.

Figure 12: Second harmonic amplitude ratio of a) single-lap joint and b) T-joint

List of Tables

Table 1: Material properties of the G250 mild steel plate

Young's Modulus (*GPa*)	205
Poisson Ratio	0.29
Density (*kg/m³*)	7870

Table 2: Material properties of the Ferroperm Pz27 Piezoceramic disc

Young's Modulus (*GPa*)	59
Poisson Ratio	0.389
Density (*kg/m³*)	7700